International Journal of Minerals, Metallurgy and Materials
Volume 25, Number 2, February 2018, Page 153
https://doi.org/10.1007/s12613-018-1558-y

Modeling study on the flow patterns of gas–liquid flow for fast decarburization during the RH process

Yi-hong Li[1,2], *Yan-ping Bao*[2], *Rui Wang*[3], *Li-feng Ma*[1], *and Jian-sheng Liu*[1]

1) Collaborative Innovation Centre of Taiyuan Heavy Machinery Equipment and School of Materials Science and Engineering, Taiyuan University of Science and Technology, Taiyuan 030024, China

2) State Key Laboratory of Advanced Metallurgy, University of Science and Technology Beijing, Beijing 100083, China

3) School of Materials Science and Engineering, North University of China, Taiyuan 030024, China

(Received: 26 April 2017; revised: 19 July 2017; accepted: 9 August 2017)

Abstract: A water model and a high-speed video camera were utilized in the 300-t RH equipment to study the effect of steel flow patterns in a vacuum chamber on fast decarburization and a superior flow-pattern map was obtained during the practical RH process. There are three flow patterns with different bubbling characteristics and steel surface states in the vacuum chamber: boiling pattern (BP), transition pattern (TP), and wave pattern (WP). The effect of the liquid-steel level and the residence time of the steel in the chamber on flow patterns and decarburization reaction were investigated, respectively. The liquid-steel level significantly affected the flow-pattern transition from BP to WP, and the residence time and reaction area were crucial to evaluate the whole decarburization process rather than the circulation flow rate and mixing time. A superior flow-pattern map during the practical RH process showed that the steel flow pattern changed from BP to TP quickly, and then remained as TP until the end of decarburization.

Keywords: modeling study; flow pattern; vacuum chamber; residence time; decarburization; RH process

1. Introduction

The production of ultra-low carbon steel has increased because of the demand of steel products with high-strength and excellent deep-draw ability. High-speed decarburization of the Ruhrstahl–Hereaeus (RH) refining equipment is an effective technology for ultra-low carbon and high-quality steel production [1]. Gas and liquid flow behavior play an important role in the steel mixing and decarburization process in the RH, as Li *et al.* [2–3] studied. Geng and Zheng [4] studied decarburization and inclusion removal in RH equipment including ladle, vacuum vessel, up-leg, and down-leg. Furthermore, the ladle bottom blowing was employed in the RH degasser, which indicated that bubbles are important for decarburization. However, the influence of characteristics of the gas–liquid flow was not given.

In terms of a chemical reactor, the RH can be regarded as an external-loop gas-lift reactor with a high efficiency of homogenization and intense mixing. Gas-lift reactors have gained much attention from researchers and numerous investigations which have been made on the characteristics of the gas–liquid two-phase flow [5–6]. The results showed that the two-phase flow patterns would influence the flow phenomena, the system stability, and the mass transfer process [7–8]. However, the fundamental research on the gas–liquid flow of the RH reactor is still insufficient in the metallurgy field and most studies focus on the steel flow phenomena, such as mixing time [9–10] and circulation flow rate [11–12]. Kato *et al.* [13] presented a quantitative investigation of the influence of the fluid flow regime, such as a perfect mixed flow, a plug flow and a non-ideal flow, in the ladle on the reaction rate. However, it did not involve the influence of fluid flow behavior, especially the gas–liquid two-phase flow in a vacuum chamber, on the reaction rate. Furthermore, the work environment of the RH equipment is different from the ordinary gas-lift reactors. That is, the pressure of the RH gas–liquid separation chamber (vacuum chamber) is much lower than the others, which induces dif-

Corresponding author: Yi-hong Li E-mail: mm.liyh@163.com

ferent flow patterns. As the vacuum chamber of the RH is the main decarburization reaction site, it is necessary to analyze the gas–liquid two-phase flow in the vacuum chamber in detail for a better understanding of the hydrodynamics and optimum operation of the reactor.

There are several difficulties in this study. First, it is difficult to measure the fluid flow characteristic in the sealed vacuum chamber. Second, due to the high flow velocity in chamber, it is difficult to capture and record the fluid flow behavior by an ordinary camera.

After the two difficulties are overcome, this work concentrates on the effect of the gas–liquid flow pattern and flow characteristics in the vacuum chamber on fast decarburization. Based on the laboratory water model experiment, the fluid behavior of the two-phase flow was monitored by a high-speed video camera and the residence time of the fluid in the chamber was tested by a conductivity meter. The flow patterns of the gas–liquid flow in the chamber and the boundaries between them were obtained. In addition, a superior flow-pattern map obtained during the practical RH process and a better evaluation index of the decarburization process were studied.

2. Experimental

2.1. Apparatus

The 300-t RH was used as a prototype to study the flow patterns in a vacuum chamber. The model of the RH was constructed with a scale factor of 1:6, by considering the dynamic and geometric similarity criteria based on the modified Froude and Reynolds numbers. Table 1 presents the main parameters of the prototype and the physical model.

Fig. 1 shows a schematic view of the physical model of the RH degasser with the tester used in the tests. Air and tap water were used as the gas and liquid phases, respectively. The water was circulated in the RH because of the density

Table 1. Dimensions of the RH system and physical parameters

Parameter	Prototype	Water model
Height of ladle / m	4.20	0.70
Up diameter of ladle / m	3.92	0.65
Down diameter of ladle / m	3.64	0.61
Steel level in ladle / m	3.92	0.65
Diameter of vacuum chamber / m	2.52	0.42
Inner diameter of snorkels / m	0.75	0.125
Outer diameter of snorkels / m	1.50	0.25
Length of snorkels / m	1.65	0.275
Gas density / ($kg \cdot m^{-3}$)	1.784	1.293
Liquid density / ($kg \cdot m^{-3}$)	7869	1000
Liquid viscosity / (Pa·s)	0.0064	0.0009

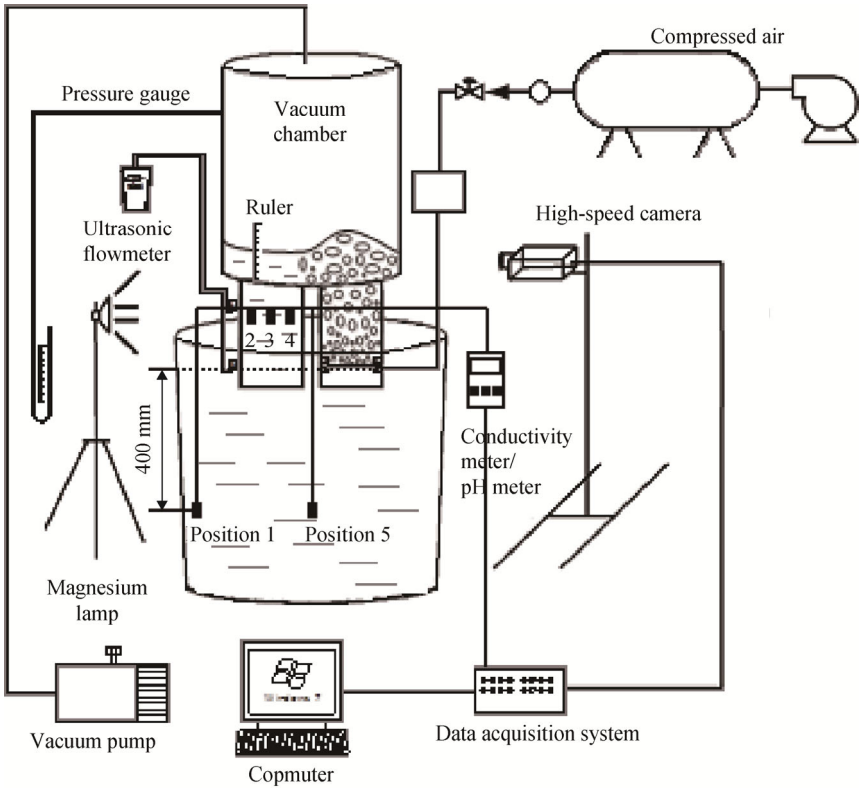

Fig. 1. Schematic diagram of the experimental set-up of the RH model.

difference between the up-leg and the down-leg. The air, supplied by a compressor, was injected into the up-leg snorkel through 16 nozzles near the bottom. The gas-flow rates were measured by gas-flow meters and controlled manually. To equally distribute the gas among the 16 nozzles, the air was first injected into the central region and finally exhausted to the atmosphere by the vacuum pump. The pressure in the vacuum chamber was monitored by a pressure gage and controlled manually. The levels of water in the vacuum chamber were controlled by a vacuum pump and measured by a ruler.

2.2. Experimental method

Two types of experiments were performed in the present work. One type was the evaluation of the fluid flow characteristics and the flow pattern, and the other type was the determination of the good flow pattern during the RH process.

2.2.1. Fluid flow characteristics

The circulation flow rate was obtained using a TDS-100H ultrasonic flow meter, as shown in Fig. 1. This flow meter is simple and with no contact with the fluid, which has no influence on the fluid flow conditions. The circulation rate was recorded every 10 s. If the circulation rate value remained relatively constant for 200 s, the flow conditions were considered as the steady state and the circulation rate was the average of the 20 values. During the experiments, the circulation flow rates of different liquid levels in the vacuum chamber were measured.

Fig. 1 also details the positions of the conductivity sensors used in the test to analyze the mixing time and the fluid residence time in the vacuum chamber. To get the mixing time, a tracer (70 mL KCl saturated solution) was injected into the vacuum chamber in pulse mode. For each operational condition simulated, changes in concentration were measured in the fixed position 1 (the distance away from the liquid level was 400 mm) by means of a conductivity meter. The flow stability of this location (400 mm away from the liquid level) was better than the other locations, which was obtained by preliminary experiments. The conductivities were continuously registered on an analog/digital PC board. Then, from the graph of the concentration as a function of time curves, one could determine the mixing time in the RH ladle (typically a 95% mixing time was normally sought). In this procedure, the mixing time at different liquid levels of the vacuum chamber was tested. For each liquid level, the measurements of mixing time were repeated five times. Removing the maximum and the minimum, the average value of the mixing time of the RH model was obtained.

To obtain the fluid residence time in the chamber, the concentration of the tracer was monitored at three different points at the exit of the chamber, as seen in Fig. 1. Then, from the concentration versus time curves, the residence time was the average of the response time of the three positions. The variations of the fluid residence time with different liquid levels were also measured in this paper.

2.2.2. Experimental decarburization time

Fig. 1 also illustrates the position of the pH sensor (pH-401) used in the test to analyze the decarburization time in the RH model. The CO_2 adsorption–desorption process was conducted for the simulation of decarburization [14], and Guo and Irons [15] mentioned that the water model of CO_2 desorption was a good tool for the simulation of carbon removal from liquid steel under reduced pressure.

In the experiments, CO_2 was injected into an aqueous solution of sodium hydroxide (NaOH) with a concentration of 0.01 mol·L^{-1}, until the pH value reached the saturation value (approximately 6.16). At this point, the operation of the RH physical model was started. For each operational condition simulated, the pH probe was fixed at position 5, as shown in Fig. 1, whose distance away from the liquid surface was equal to that of position 1. Furthermore, there was no significant difference in pH value at different locations of the pH sensor [16]. The variation of pH value was monitored during the entire test.

The total CO_2 content was determined through monitoring the pH values. Thus, the CO_2 concentration (c_{CO_2}) in the solution can be described as [17]

$$c_{CO_2} = \left(10^{-pH} + c_{NaOH} - \frac{K_{H_2O}}{10^{-pH}}\right) \times \frac{K_1K_2 + K_1 \cdot 10^{-pH} + 10^{-2pH}}{2K_1K_2 + K_1 \cdot 10^{-pH}} \quad (1)$$

where c_{NaOH} is the initial concentration of the caustic soda solution, mol·L^{-1}; K_{H_2O} is the ionic product of water, equal to 10^{-14}; $K_1 = 10^{-6.352}$ and $K_2 = 10^{-10.329}$ are the first and secondary ionization constants of carbonic acid, respectively [18].

The CO_2 concentration versus time curves were constructed and the time used was called the simulated time or decarburization time of the RH model (t_m). According to the modified Froude number, the relationship between the decarburization time of the model t_m and the actual decarburization time t_p could be deduced as

$$\frac{t_m}{t_p} = \lambda^{0.5} \cdot \frac{\rho_{lp}}{\rho_{lm}} \cdot \frac{\rho_{gm}}{\rho_{gp}} = 2.33 \quad (2)$$

where λ is the scale factor between the model and the pro-

totype; ρ_g is the gas density, kg·m^{-3}; ρ_l is the liquid density, kg·m^{-3}; subscripts m and p represent the model and the prototype, respectively.

According to Eq. (2), t_m was calculated as the average value of the practical decarburization time (t_p) at which the carbon content reached the ultra-low level in the actual RH process. Based on the CO_2 concentration versus time curves in the experiments, when the time reached t_m, the corresponding CO_2 concentration was defined as the experimental ultimate concentration. So, for each operational condition simulated, the experimental decarburization time t_e was measured from the start to the time taken to obtain the experimental ultimate concentration. Also, t_e expressed the required time in which the CO_2 concentration reduced from its initial value to above the minimum value under different simulation conditions.

2.2.3. Flow pattern in the vacuum chamber

The fluid behavior of the two-phase flow was observed by a high-speed video camera (Fastec HiSpec5) with a high speed of 1267 frames per second. A magnesium lamp was utilized for illumination. During the experiments, images of the flow patterns of the vacuum chamber were captured at different liquid levels in the chamber and different flow rates of the injection gas (Fig. 1). Then, the images were reproduced in slow motion for estimating the flow pattern for each experimental condition.

2.2.4. Gas holdup in the vacuum chamber

The flow-pattern transition point can be identified from the slope changes of the gas holdup [19]. It was observed that there was little entrainment of gas bubbles in the down-leg of the vacuum chamber; hence, the measured gas holdup was the overall gas holdup in the up-leg [20].

The overall gas holdup β was calculated from the unaerated liquid height H_L and the aerated liquid height H_M by [19]

$$\beta = 1 - \frac{H_L}{H_M} \tag{3}$$

3. Results and discussion

3.1. Evaluation index for the flow behavior

Mixing time and circulation flow rate in a RH vessel have been the subjects of several studies. Most investigations [21–24] provided the following conclusions: a large circulation flow rate and a short mixing time would increase the decarburization rate, and the relationship between the circulation rate and the structural parameters of the RH is given by

$$Q = K \cdot Q_g^a \cdot D_u^b \cdot H_i^c \cdot D_g^d \tag{4}$$

where Q is the circulation flow rate, t·min^{-1}; Q_g is the gas flow rate of Ar, L·min^{-1}; D_u is the inner diameter of snorkels, m; H_j is the immersion depth of snorkels, m; D_g is the inner diameters of gas port, m; K is the coefficient; a, b, c, and d are constants determined by the experiments.

In Eq. (4), the effect of structural parameters on mixing and decarburization were researched, and the decarburization efficiency was indeed improved through optimizing the structural parameters. But, could the mixing time and circulation flow rate comprehensively evaluate the whole RH process?

The mixing time, circulation flow rate, and liquid residence time in the chamber along with the change of liquid level in the chamber were measured and plotted in Fig. 2. Besides, based on Table 2, the variation of the experimental decarburization time t_e with the liquid levels is also shown in Fig. 2(a). Due to the importance of decarburization in the RH process, the comparison between the experimental decarburization time and the evaluation indicators at different liquid levels in the chamber was displayed in Fig. 2.

From Figs. 2(a) and 2(b), at the given RH and Ar gas-flow rate, when the liquid level was lower than 6 cm, the decarburization time decreased with increasing circulation flow rate. When the liquid level was higher than 6 cm, the decarburization time increased greatly while the circulation flow rate changed slowly. These results indicated that the circulation flow rate accurately evaluated the RH process in a certain range and it was not applicable for the whole process. The comparison between Figs. 2(a) and 2(c) also showed the similar situation, when the liquid level was higher than 8 cm, the mixing time was not the main influential factor of the decarburization time. Thus, the circulation flow rate and the mixing time were not applicable for evaluating the whole process.

Since the vacuum chamber was the main decarburization site, the decarburization time was used to evaluate the assessment criteria of the fluid's characteristics. As shown in the comparison between Figs. 2(a) and 2(d), during the whole process the decarburization time decreased with increasing liquid residence time and increased with decreasing liquid residence time. Therefore, the liquid residence time was the most important indicator for evaluating the decarburization process and it should be first considered to evaluate the fluid behavior during the RH process. In addition, to acquire the fast decarburization rate, there should be a larger reaction area for the residence time, so the reaction area should also be considered to estimate the behavior of the fluid.

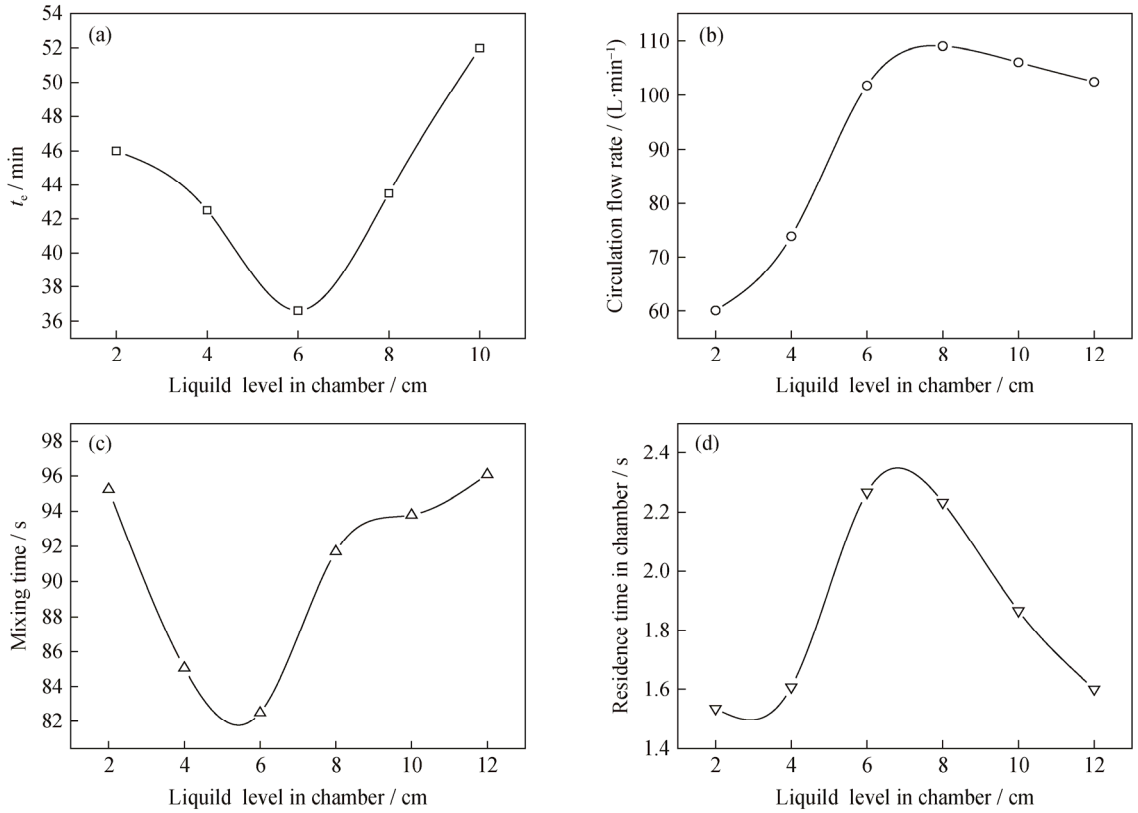

Fig. 2. Decarburization time t_e (a), circulation flow rate (b), mixing time (c), and liquid residence time (d) at different liquid levels in the chamber.

Table 2. Steps to get the experimental decarburization time

Step	Parameter	Result	Note
1	t_p / min	17.0	The average value of the practical decarburization time at which the carbon content is reduced to 10–15 ppm in Shougang Jingtang United Iron and Steel Co. Ltd (SJTISC).
2	t_m / min	40.0	The decarburization time of the RH model was obtained by $t_m = 2.33t_p$ (Eq. (2)).
3	Experimental ultimate CO_2 concentration / (mol·L^{-1})	0.015	When the time reached 40.0 min, select the smallest value of CO_2 concentration (Eq. (1)) under different experimental conditions.
4	t_e / min	Fig. 2(a)	The time of CO_2 concentration reduced from the initial value to 0.015 mol·L^{-1} under different simulation conditions.

3.2. Flow pattern in the vacuum chamber

The hydrodynamic behavior of gas-lift reactors strongly depends on the gas–liquid flow pattern [25]. The schematic of the flow pattern is illustrated in Fig. 3 through visual observation of different flow patterns which occurred in the vacuum chamber. The schematic showed that there were three flow patterns with different bubbling characteristics and steel surface states. The boiling pattern (BP) is that some splash droplets existed in the chamber and a sharp fluctuation arose above the up-leg snorkel as well as the bubbles were concentrated. The transition pattern (TP) is that a small number of splash droplets existed and the bubbles became dispersed. The wave pattern (WP) is that no splash droplets existed and a sharp fluctuation occurred at all the fluid surfaces of the vacuum chamber, and some diffuse bubbles also existed next to the fluid surface. The typical photographs of the flow patterns in the vacuum chamber of the RH, in good accordance with Fig. 3, are shown in Fig. 4. The photographs were captured at the liquid level in the chamber varying from 2 to 8 cm (12 to 48 cm in actual production) and changing gas-flow rates. From Fig. 4, it was obvious that the splash region was decreased with the increasing liquid level, and the effect of the liquid level on the flow pattern was more significant than that of the gas-flow rate.

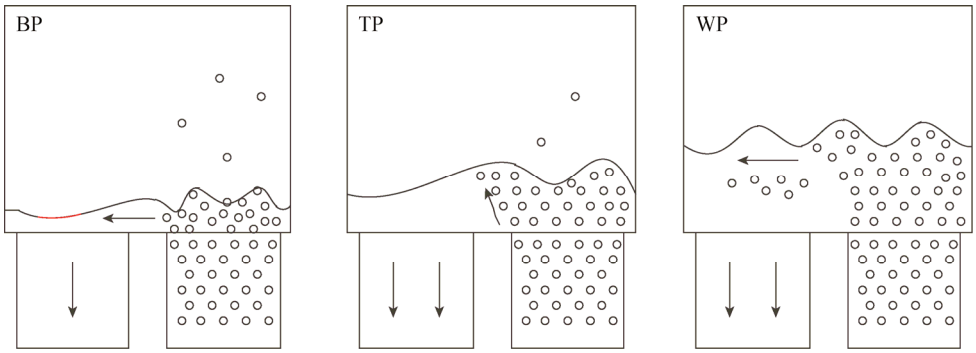

Fig. 3. A sketch of the flow patterns in the vacuum chamber (the arrows represent the flow direction of steel).

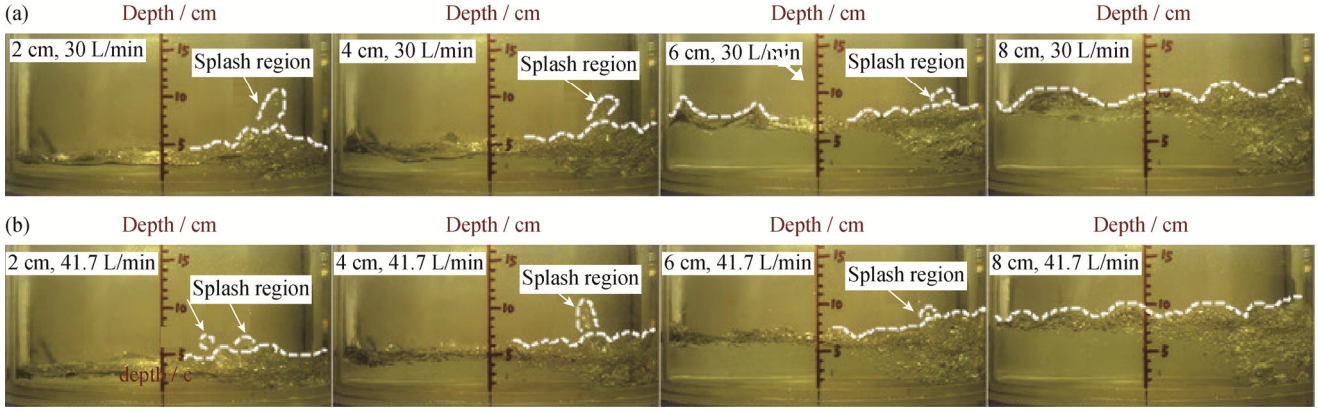

Fig. 4. Flow patterns of different steel levels at different gas-flow rates: (a) 30 L·min^{-1}; (b) 41.7 L·min^{-1}.

The reason for the existence of three flow patterns can be analyzed as follows. The BP existed at low liquid levels which led to low liquid circulation rates and small amounts of liquid in the chamber. This low velocity and small amount of liquid caused the low density of the gas–liquid fluid. Furthermore, the low-density fluid was easy to generate splash droplets because of the low surface tension. With increased liquid levels, the gas–liquid surface tension was increased with the driving force of faster liquid circulation. When the bubble was split into many small bubbles by increasing the fluid speed, the fluid flow entered the TP. The WP was found at the high-liquid level which was caused by the low pressure in the chamber; this low pressure led to the high differential pressure which increased the liquid fluctuation.

Moreover, the flow regime transition had a significant effect on the liquid velocity in the down-leg regardless of the gas injection mode [19]. This influence was indirectly reflected in the gas holdup changes and the unaerated liquid level significantly affected the transition [5]. Thus, the flow-pattern transition point can be identified from the slope changes of the gas holdup along with the liquid level.

The effect of the liquid level on the average gas holdup in the vacuum chamber is shown in Fig. 5, where the gas holdup decreased with increasing liquid level at a given lifting gas-flow rate. This is because with an increase in liquid height, the liquid circulation velocity increased, which in turn, caused a decrease in residence time of the gas bubbles and a decrease in gas holdup. Similar results were reported by Seigel *et al.* [26] and Merchuk *et al.* [27]. Therefore, at lower liquid levels, more bubbles collected in the chamber at the given gas-flow rate which caused a smaller density of gas–liquid flow and smaller surface tension. In this case, BP was generated. At higher liquid levels, less bubbles collected because of the fast circulation rate which brought the low gas holdup. During WP, due to the limited effectiveness of

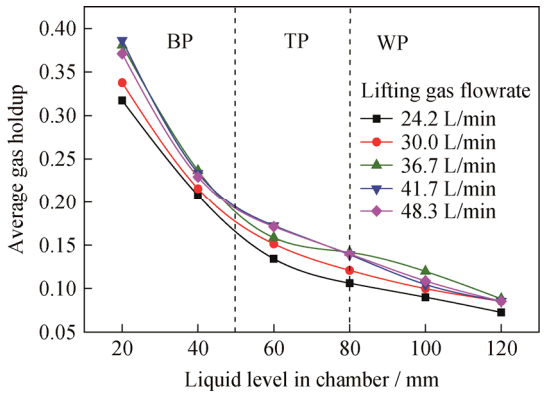

Fig. 5. Variations of gas holdup with liquid levels and lifting gas flowrate.

increasing the liquid level to increasing the circulation rate, the change rate of gas holdup became small. Therefore, the liquid level for the transition from BP to TP was 5 cm and the transition point between TP and WP was 8 cm.

3.3. Evaluation of different flow patterns

3.3.1. Residence time of steel in the vacuum chamber

The three stages of decarburization reaction were the nucleation of CO, the growth of CO bubbles, and the discharge of CO gas [28]. Due to the complete running of these stages, the carbon content of steel would reach an ultra-low level.

Assuming the homogenous nucleation of CO bubbles occurred when the pressure of the chamber was less than 10 kPa and the bubbles could be discharged when it grew up to 5 mm in diameter. According to the calculation, the number of molecules needed for nucleation of CO bubbles was 6.20×10^9 and the number of molecules needed for a 5-mm CO bubble was 5.10×10^{20}. In the practical RH process, when the CO bubbles grew to 5 mm, the carbon content would be decreased by 1.34 ppm in 3.22 s, because the carbon content, on average, was reduced by 50 ppm in 2 min with the 300-t RH of SJTISC. So, the residence time should be more than 3.22 s for deep decarburization. Here, we did not consider the time of mass transfer. However, if the steel stayed in the chamber too long, the reaction became difficult because of the very low element content. Thus, the residence time should be accurately controlled.

According to the visual observation of the fluid's behavior and the measurement results of the residence time, the sketch of the fluid's flow path in the vacuum chamber was obtained, as shown in Fig. 6, and the qualitative residence time could be deduced from it. Based on the qualitative residence time, the evaluation results of three flow patterns were summarized as below.

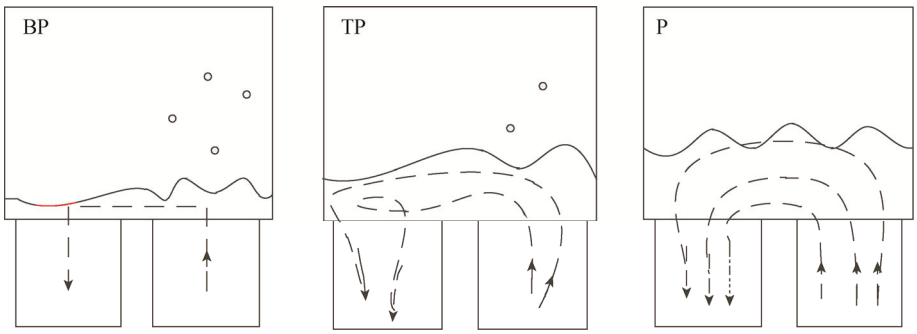

Fig. 6. Sketch of the fluid flow behavior in the vacuum chamber (the arrows represent the flow direction of steel).

When the flow pattern was the BP, the amount of fluid in the vacuum chamber was small, and the fluid directly flowed out from the down-leg after flowing into the chamber. Hence, the residence time was short and the fluid would be circulated many times to finish the treatment of the 300-t steel. There was no doubt that the decarburization time was increased at the BP. Besides, the amount of cold steel stuck on the refractory was increased because of more splash droplets. When the flow pattern was TP, the residence time was increased with the increasing flow path which was caused by the increasing fluid volume. Hence, TP was the desirable flow pattern for fast and deep decarburization with small amounts of cold steel. When the flow pattern was WP, the residence time was less than that of TP because part of the fluid in the vacuum chamber directly flowed out from the down-leg after flowing into the chamber. In addition, when the liquid level was high, the reaction area was decreased because the reaction site came close to the liquid surface [29–30] (detailed explanation is provided in the next section). Hence, WP could not provide an effective reaction environment for fast decarburization.

3.3.2. Reaction area

The following places can be considered as reaction sites [28]: (1) interfaces (S_{gas}) between the molten steel and the Ar bubbles injected into the snorkel; (2) free surface ($S_{surface}$) of the molten steel in the vacuum chamber (this free surface included splashes); (3) bubbles of carbon monoxide formed by the decarburization reaction ($S_{[C]+[O]}$). These reaction sites are summarized as

$$S_T = S_{gas} + S_{[C]+[O]} + S_{surface} \quad (5)$$

However, which reaction mechanism contributed more to the fast decarburization rate? Takahashi *et al.* [31] found that the contribution of CO bubbles to the decarburization was the greatest. But Kitamura *et al.* [32] obtained that the decarburization reaction proceeded on the bath surface (90%), the CO gas bubble (8%) and the injected gas bubble (2%). Practically, it was impossible to distinguish one decarburization from another. In short, the larger the reaction area, the faster the decarburization rate.

The reaction area was indirectly obtained by the reaction

depth. Here, the reaction depth expressed the height of the reaction region, which meant that the height was from the location of the carbon–oxygen reaction to the steel surface in the vacuum chamber. A high reaction depth represented a large reaction area. The expression of decarburization reaction depth h_r was deduced based on the equilibrium constant $K^{\ominus}$ (Eq. (6)) and partial pressure of the CO gas (Eq. (7)) [28]. As shown in Eq. (8), the variation of reaction depth during the process could be obtained by the carbon and oxygen contents and the pressure of the vacuum chamber. These data were from the practical process.

$$K^{\ominus} = \frac{p_{CO} / p^{\ominus}}{\omega[C] \cdot \omega[O]} \tag{6}$$

$$p_{CO} \geq p_V + \rho g h + 2\sigma / r \tag{7}$$

$$h_r = 1.45(0.872 K^{\ominus} \cdot \omega[C] \cdot \omega[O] - p_V / 101325) \tag{8}$$

where $K^{\ominus}$ is the equilibrium constant of the reaction between carbon and oxygen; T is the temperature, K; p_{CO} is the partial pressure of CO gas, Pa; $p^{\ominus}$ is the standard atmospheric pressure, 101325 Pa, p_V is the pressure of the vacuum chamber, Pa, h is the height of liquid steel in the vacuum chamber, m; σ is the surface tension, $N \cdot m^{-1}$; r is the average diameter of bubbles, m; h_r is the decarburization reaction depth, m; $\omega[C]$ is the mass fraction of carbon content, wt%; $\omega[O]$ is the mass fraction of oxygen content, wt%; and g is the acceleration of gravity, m^2/s.

The variation of reaction depth and the steel level of the real vacuum chamber with the changing actual time are shown in Fig. 7. The reaction depth was rapidly reduced from 0.8 to 0.1 m and the steel level was increased from 0 to 0.12, 0.5 m or higher. The highest steel level changed with the snorkel length and the immersion depth. The reaction depth was compared with the liquid-steel level, as shown in Fig. 7, and when the liquid-steel level was lower than the reaction depth, the reaction occurred in the whole region of the vacuum chamber; when the liquid-steel level was higher than the reaction depth, the decarburization turned into the partial region reaction. The reaction sites shifted to the surface of the chamber in the late decarburization process because of the high steel level and low reaction depth. As analyzed above, different steel levels resulted in different flow patterns in the vacuum chamber, so we could determine which flow pattern was better for increasing the reaction area.

As an example, the immersion depth of the real RH was 700 mm, as shown in Fig. 7. The steel level was increased from 0 to 480 mm (from 0 to 8 cm in the experimental chamber), which meant the flow pattern changed from BP to WP. Hence, the all-region reaction occurred in both BP and TP, and the partial region reaction occurred in WP; this phenomenon was similar to the flow condition displayed in Fig. 8. In BP, due to the small amount of liquid steel and the low gas-flow rate in the chamber, the reaction area was limited although the reaction occurred in the whole region. In TP, the liquid-steel volume increased by more than 50% and the Ar bubbles increased for high gas-flow rates, so the reaction area was greater than that of BP. In WP, the amount of steel for the reaction was decreased and the reaction on Ar bubbles was restricted by the mass transfer because of the relatively low carbon and oxygen contents. Thus, the reaction area was smaller than that of TP.

Consequently, for a given reactor, the flow pattern was important for the residence time and the reaction area and was mainly determined by the liquid-steel level in the vacuum chamber. The TP was desired in a reactor for the long residence time and large reaction area and would lead to fast and deep decarburization.

3.4. A superior flow-pattern map during the practical RH process

In actual production, changes in liquid steel with different decarburization times and different pressures in the vacuum chamber are shown in Fig. 9. With an increase in decarburization time, the liquid level was increased with the decreasing pressure of the chamber. When the pressure decreased to 67 Pa, the liquid level reached the highest value. In this work, the highest steel level of the study subject was 250 mm (Fig. 9(a)). If the immersion depth was increased to 650 mm (Fig. 9(b)) and the snorkel length was reduced to 1450 mm (Fig. 9(c)), the highest steel level would increase to 450 and 650 mm, respectively. This steel level variation caused different flow patterns in the vacuum chamber. To improve the decarburization rate, it was necessary to analyze the change of the flow pattern and optimize the flow-pattern map during the decarburization process.

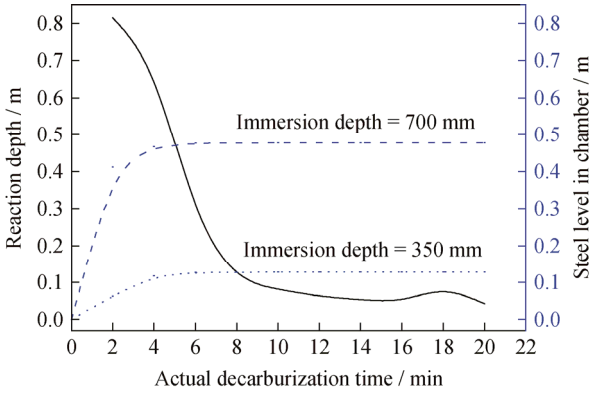

Fig. 7. Variations of the reaction depth and the real steel level of the chamber as a function of decarburization time.

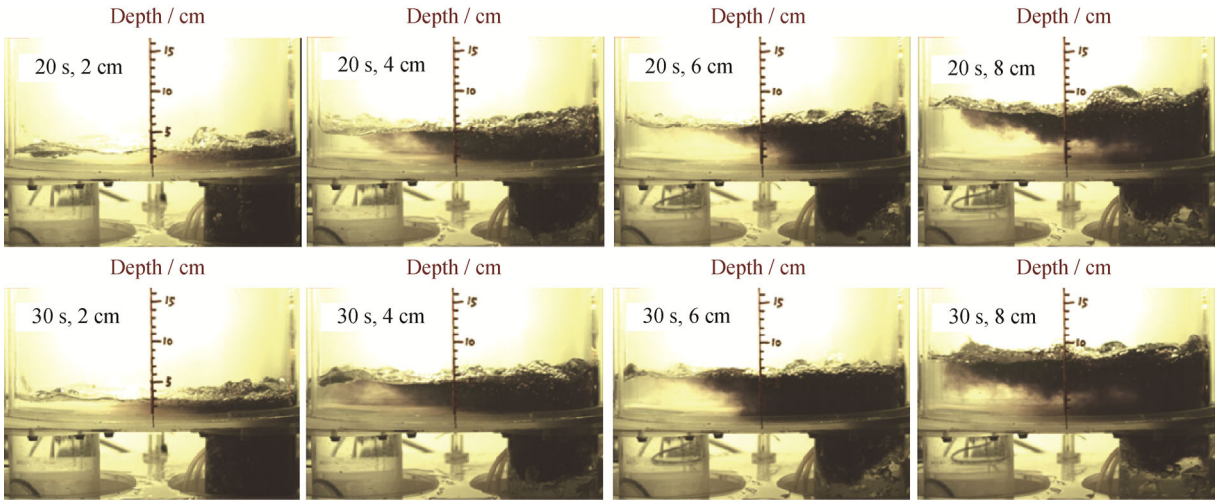

Fig. 8. Photographs of the fluid flow path in the vacuum chamber.

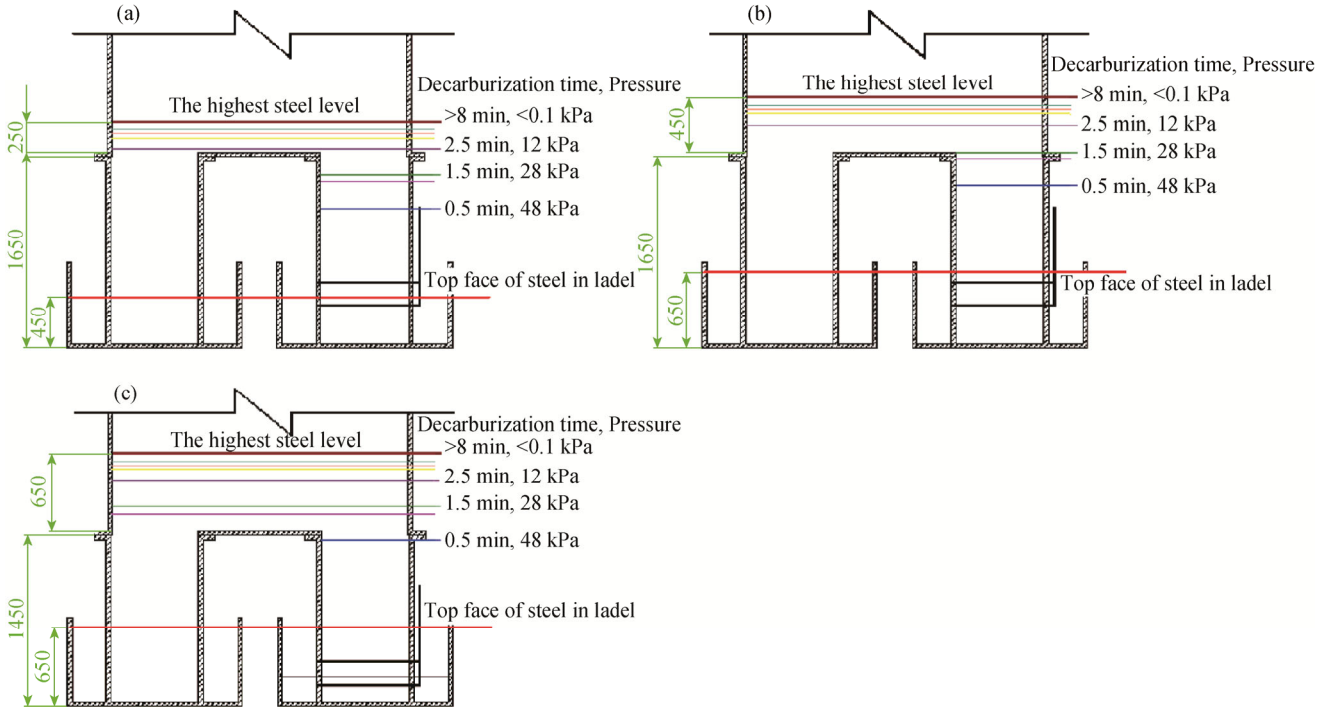

Fig. 9. Changes over time in liquid steel with different pressures of the vacuum chamber (the unit of length is mm).

According to the experimental results of the flow-pattern boundaries, the flow-pattern map during the practical decarburization process could be described as follows. From Fig. 9(a), in the vacuum chamber, there was no steel for 2.5 min after the start of decarburization, so the splash droplets and Ar bubbles became the main reaction site. After 2.5 min, the steel began to flow into the chamber and the steel circulated immediately. However, the highest steel level (250 mm) was equivalent to 4 cm or so in the experimental chamber. In other words, the steel flow pattern was BP until the end of decarburization, which limited the decarburization rate.

Since it was often desirable to operate under the TP, it was most important to accurately control the steel level in the vacuum chamber. From Fig. 9(b), the steel began to circulate at 1.5 min and the steel level reached 271 mm (4.5 cm in the water model) at 2.5 min. The highest steel level (450 mm) was equivalent to 7.5 cm in the experimental chamber. That is, the steel flow pattern was BP in the first 2.5 min, and then the steel flow entered TP and retained this pattern for almost the remainder of the decarburization time. Under this condition, the decarburization rate would become larger. However, considering Fig. 9(c), what would happen if the immersion depth continued to increase or the snorkel

length continued to decrease? Then, the steel began to circulate after 0.5 min and the steel level reached 242 mm (4.0 cm in the water model) at 1.5 min. In the next minute, the steel level reached 471 mm (7.9 cm in the water model) quickly. This meant that TP lasted for less than 1 min, which was not conducive to fast decarburization.

Consequently, to attain a fast decarburization rate, the steel flow pattern should change from BP to TP quickly, and then remain at TP until the end of decarburization during the practical RH process. A superior flow-pattern map can be used as an optimization criterion of the process parameters.

4. Conclusions

The effect of steel flow patterns in a vacuum chamber on fast decarburization was studied using a water model and a high-speed video camera, and the evaluation indicators of the whole decarburization process were redefined. The following conclusions, which can be applied for a large (300 t) RH degasser, were obtained.

(1) The circulation flow rate and the mixing time were not applicable for evaluating the whole RH process. The liquid residence time in the vacuum chamber was the most important indicator and should be first considered to evaluate the fluid behavior during the RH process.

(2) There were three flow patterns: the BP in which some splash droplets existed in the chamber and a sharp fluctuation arose above the up-leg snorkel; the TP in which a small number of splash droplets existed and the bubbles became dispersed; and the WP in which no splash droplets existed and a sharp fluctuation occurred at all the fluid surfaces in the vacuum chamber, some diffuse bubbles also existed next to the fluid surface.

(3) The flow pattern transformed from BP to TP until the actual liquid level was higher than 30 cm, and the transition point between TP and WP was larger than 48 cm. Because of the long residence time and large reaction area, TP was so desirable in a RH reactor that fast and deep decarburization could be realized.

(4) To obtain a fast decarburization rate, the steel flow pattern should change from BP to TP quickly, and then remain at TP until the end of decarburization during the practical RH process. A superior flow-pattern map can be used as an optimization criterion of the process parameters.

Acknowledgements

This work was financially supported by the National Natural Science Foundation of China (No.51704203), the PhD Early Development Program of Taiyuan University of Science and Technology (Nos. 20152008, 20152013, and 20152018), Shanxi Province Science Foundation for Youths (No. 201601D202027), Key Project of Research and Development Plan of Shanxi Province (Nos. 201603D111004 and 201603D121010), and NSFC-Shanxi Coal Based Low Carbon Joint Fund (No. U1510131).

References

[1] Y. Fukuda, S. Onoyama, T. Imai, S. Mukawa, T. Sado, K. Fukiage, O. Kunitake, N. Takagi, and H. Matsumoto, Development of high-grade steel manufacturing technology for mass production at Nagoya works, *Nippon Steel Tech. Rep.*, 2013, No. 104, p. 90.

[2] Y.H. Li, Y.P. Bao, R. Wang, M. Wang, Q.X. Huang, and Y.G. Li, Modeling on liquid level and bubble behavior in vacuum chamber of RH process, *J. Iron Steel Res. Int.*, 23(2016), No. 4, p. 305.

[3] Y.H. Li, Y.P. Bao, M. Wang, R. Wang, and D.C. Tang, Influence of process conditions during Ruhrstahl-Hereaeus refining process and effect of vacuum degassing on carbon removal to ultra-low levels, *Ironmaking Steelmaking*, 42(2015), No. 5, p. 366.

[4] D.Q. Geng, J.X. Zheng, K. Wang, P. Wang, R.Q. Liang, H.T. Liu, H. Lei, and J.C. He, Simulation on decarburization and inclusion removal process in the Ruhrstahl–Heraeus (RH) process with ladle bottom blowing, *Metall. Mater. Trans. B*, 46(2015), No. 3, p. 1484.

[5] L.J. Luo, J.Q. Yuan, P. Xie, J.W. Sun, and W. Guo, Hydrodynamics and mass transfer characteristics in an internal loop airlift reactor with sieve plates, *Chem. Eng. Res. Des*., 91(2013), No. 12, p. 2377.

[6] T.T. Xu, X.D. Jiang, N. Yang, and J.H. Zhu, CFD simulation of internal-loop airlift reactor using EMMS drag model, *Particuology*, 19(2015), No. 2, p. 124.

[7] C. Kamata and K. Ito, Cold model experiments on the application of gas lift pump to the transportation of molten metal, *ISIJ Int.*, 35(1995), No. 7, p. 859.

[8] J. Yue, G.W. Chen, Q. Yuan, L.G. Luo, and Y. Gonthier, Hydrodynamics and mass transfer characteristics in gas–liquid flow through a rectangular microchannel, *Chem. Eng. Sci*., 62(2007), No. 7, p. 2096.

[9] M.K. Mondal, N. Maruoka, S. Kitamura, G.S. Gupta, H. Nogami, and H.Shibata, Study of fluid flow and mixing behavior of a vacuum degasser, *Trans. Indian Inst. Met.*, 65(2012), No. 3, p. 321.

[10] L.F. Zhang and F. Li, Investigation on the fluid flow and mixing phenomena in a Ruhrstahl-Heraeus (RH) steel degasser using physical modeling, *JOM*, 66(2014), No. 7, p. 1227.

[11] B.H. Zhu, Q.C. Liu, D. Zhao, S. Ren, M.R. Xu, B.C. Yang, and B. Hu, Effect of nozzle blockage on circulation flow rate in up-snorkel during the RH degasser process, *Steel Res. Int.*, 87(2016), No. 2, p. 136.

[12] D. Mukherjee, A.K. Shukla, and D.G. Senk, Cold model-based investigations to study the effects of operational and nonoperational parameters on the Ruhrstahl–Heraeus degassing process, *Metall. Mater. Trans. B*, 48(2017), No. 2, p. 763.

[13] Y. Kato, H. Nakato, T. FJii, S. Ohmiya, and S. Takatori, Fluid flow in ladle and its effect on decarburization rate in RH degasser, *ISIJ Int.*, 33(1993), No. 10, p. 1088.

[14] Q.X. Rui, F. Jiang, Z.M. Ma, Z.M. You, G.G. Cheng, and J. Zhan, Effect of elliptical snorkel on the decarburization rate in single snorkel refining furnace, *Steel Res. Int.*, 84(2013), No. 2, p. 192.

[15] D. Guo and G.A. Irons, Modeling of gas–liquid reactions in ladle metallurgy: Part I. Physical modelling, *Metall. Mater. Trans. B*, 31(2000), No. 6, p. 1447.

[16] L. Neves, H.P.O. de Oliveria, and R.P. Tavares, Evaluation of the effects of gas in the vacuum chamber of a RH degasser on melt circulation and decarburization rates, *ISIJ Int.*, 49(2009), No. 8, p. 1141.

[17] S. Inada and T. Watanabe, A study of the effects of CO_2 absorption in the NaOH solution–CO_2 gas jet model, *Tetsu-to-Hagané*, 62(1976), No. 7, p. 807.

[18] S.H. Kim and R.J. Fruehan, Physical modeling of liquid/liquid mass transfer in a gas stirred ladle, *Metall. Trans. B*, 18(1987), No. 2, p. 381.

[19] L.J. Luo, F.N. Liu, Y.Y. Xu, and J.Q. Yuan, Hydrodynamics and mass transfer characteristics in an internal loop airlift reactor with different spargers, *Chem. Eng. J.*, 175(2011), No. 1, p. 494.

[20] Y.X. Guo, M.N. Rathor, and H.C. Ti, Hydrodynamics and mass transfer studies in a novel external-loop airlift reactor, *Chem. Eng. J.*, 67(1997), No. 3, p. 205.

[21] L. Lin, Y.P. Bao, F. Yue, L.Q. Zhang, and H.L. Ou, Physical model of fluid flow characteristics in RH-TOP vacuum refining process, *Int. J. Miner. Metall. Mater.*, 19(2012), No. 6, p. 483.

[22] F. Ahrenhold and W. Pluschkell, Circulation rate of liquid steel in RH degassers, *Steel Res.*, 69(1998), No. 2, p. 54.

[23] X.G. Ai, Y.P. Bao, W. Jiang, and J.H. Liu, P.H. Li, and T.Q. Li, Periodic flow characteristics during RH vacuum circulation refining, *Int. J. Miner. Metall. Mater.*, 17(2010), No. 1, p. 17.

[24] J.H. Wei, N.W. Yu, Y.Y. Fan, S.L. Yang, J.C. Ma, and D.P. Zhu, Study on flow and mixing characteristics of molten steel in RH and RH-KTB refining processes, *J. Shanghai Univ.*, 6(2002), No. 2, p. 167.

[25] N. Bendjaballah, H. Dhaouadi, S. Poncin, N. Midoux, J.M. Hornut, and G. Wild, Hydrodynamics and flow regimes in external loop airlift reactors, *Chem. Eng. Sci.*, 54(1999), No. 21, p. 5211.

[26] M.H. Siegel, J.C. Merchuk, and K. Schugerl, Air-lift reactor analysis: Interrelationships between riser, downcomer, and gas–liquid separator behavior, including gas recirculation effects, *AIChE J.*, 32(1986), No. 10, p. 1585.

[27] J.C. Merchuk , N. Ladwa, A. Cameron, M. Bumler, and A. Pickett, Concentric-tube airlift reactors: effect of geometrical design on performance, *AIChE J.*, 40(1994), No. 7, p. 1105.

[28] X.H. Huang and J.Z. Li, *Principles of Steel Metallurgy*, Metallurgical Industry Press, Beijing, 2013, p. 497.

[29] S.Y. Kitamura, H. Aoki, K.I. Miyamoto, H. Furuta, K. Yamashita, and K. Yonezawa, Development of a novel degassing process consisting with single large immersion snorkel and a bottom bubbling ladle, *ISIJ Int.*, 40(2000), No. 5, p. 455.

[30] N. Maruoka, F. Lazuardi, H. Nogami, G.S. Gupta, and S.Y. Kitamura, Effect of bottom bubbling conditions on surface reaction rate in oxygen–water system, *ISIJ Int.*, 50(2010), No. 1, p. 89.

[31] M. Takahashi, H. Matsumoto, and T. Saito, The mechanism of decarburization in RH degasser, *ISIJ Int.*, 35(1995), No. 12, p. 1452.

[32] T. Kitamura, K. Miyamoto, R. Tsujno, S. Mizoguch, and K. Kato, Mathematical model for nitrogen desorption and decarburization reaction in vacuum degasser, *ISIJ Int.*, 36(1996), No. 4, p. 395.